SPE-194323-MS

Integrated Analysis of the Coupling Between Geomechanics and Operational Parameters to Optimize Hydraulic Fracture Propagation and Proppant Distribution

Ankush Singh, Shaochuan Xu, and Mark Zoback, Stanford University; Mark McClure, ResFrac Corporation

This paper was prepared for presentation at the SPE Hydraulic Fracturing Technology Conference and Exhibition held in The Woodlands, Texas, USA, 5-7 February 2019.

Abstract

This paper presents an analysis of the interactions between stimulation design and two important geomechanical effects: the variation of least principal stress (S_{hmin}) between lithological layers and the stress shadow effect that arises from simultaneously propagating adjacent hydraulic fractures. To demonstrate these interactions, hydraulic fracture propagation is modeled with a 5-layer geomechanical model representing an actual case study. The model consists of a profile of S_{hmin} measurements made within, below and above the producing interval. The stress variations between layers leads to an overall upward fracture propagation and proppant largely above the producing interval. This is due to interactions between the pressure distribution within the fracture and the stress contrast in the multiple layers. A sensitivity study is done to investigate the complex 3-D couplings between geomechanical constraints and well completion design parameters such as landing zone, cluster spacing, perforation diameter, flow rate and proppant concentration. The simulation results demonstrate the importance of a well characterized stress stratigraphy for prediction of hydraulic fracture characteristics and optimization of operational parameters.

Introduction

Simultaneous propagation of multiple hydraulic fractures in close vicinity during plug-and-perf operations is influenced by wellbore effects (completion design parameters such as stage length, perforation diameter and perforation cluster spacing), fluid effects (pumping rate, fracturing fluid viscosity), in-situ stress variations within, above and below the producing interval, and stress shadowing between propagating fractures from each perforation cluster. This paper presents a sensitivity analysis based on an actual case study to illustrate the complex 3-D couplings among these important factors that control successful stimulation optimization.

Papers documenting variations of S_{hmin} with depth from one lithofacies to another are ubiquitous in unconventional reservoirs. The variation of stress with depth and lithology is also well documented for the Piceance Basin in Colorado (Warpinski et al. 1985). Fisher and Warpinski (2012) consider stress layering to be the most important parameter in determining fracture height and containment. Xu and Zoback (2015) show data on the variation of the least principal stress with depth at a site in the Permian Basin and argue

that viscoelastic stress relaxation caused an increase in the S_{hmin} in the Wolfcamp formation compared to the Spraberry formation. Ma and Zoback (2017) observed a variation in S_{hmin} between different stages for a well in the Woodford shale, where the stages associated with high clay and organic content lithofacies show an increase in S_{hmin}. They also correlated the S_{hmin} variations to stimulation performance. Alalli and Zoback (2018) attributed horizontal fractures in the organic rich lower Marcellus shale to increase in S_{hmin} caused by viscoelastic stress relaxation.

Stress shadow effects play a significant role in the interaction between multiple hydraulic fractures. The stress shadow effect results from alteration of the stress due to the mechanical opening of the hydraulic fracture and poroelastic effects. The outward fluid pressure in the fracture compresses adjacent formation, in the direction normal to the fracture face, thereby increasing S_{hmin} (Soliman et al. 2008; Daneshy 2014; Warpinksi et al. 2013). The increased stress due to this effect prevents the growth of closely spaced hydraulic fractures often leading to failed perforation clusters (Fisher et al. 2004; Wheaton et al. 2014). For a single isolated stage, stress shadow effects tend to favor propagation of outer fractures while restricting growth of inner fractures during stimulation (Wheaton et al. 2014; Agarwal et al. 2012).

A number of fluid flow effects within the wellbore including wellbore friction, perforation pressure drop, proppant settling have a significant impact on distribution of fracture fluid within the perforation clusters. The purpose of a limited entry design is to ensure a uniform distribution of flow across the perforation clusters by utilizing the perforation pressure drop as a flow limiting mechanism for individual clusters. The perforation pressure drop is related to the perforation size, number of perforations in the cluster and flow rate (Veatch 1983; Cramer 1987). This results in a competing mechanism between the stress shadow effect and the limited entry effects. Adequate perforation pressure drop can increase the probability of propagation from all the clusters.

Model set up

The interactions between the geomechanical effects and operational parameters is tested using a 5-layer idealized geomechanical model corresponding to an actual case study. The key geomechanical parameters are shown in Table 1. The layer thicknesses and measured values of S_{hmin} from DFITs correspond to the actual case study. The porosity, permeability and Young's modulus values have been assumed to be reasonable and homogenous throughout the rock volume. The stress measurements are made close to the center of each layer. The stress within each layer is assumed to follow a depth gradient (Figure 1). This assumption is tested by comparing the results to a realization which assumes a constant S_{hmin} per layer. All the layers are assumed to be saturated with gas and a small residual water saturation.

Table 1—Key geomechanical parameters for the model

Layer	Top Depth (ft.)	Bottom Depth (ft.)	Measured S_{hmin} (psi)	Permeability Horizontal (md)	Permeability Vertical (md)	Porosity (%)	Young's Modulus (psi)
A	9500	10010	10440	5.00E-05	0	5	4000000
B	10010	10250	10000	5.00E-05	0	5	4000000
C	10250	10497	10590	5.00E-05	0	5	4000000
D	10497	10582	11080	5.00E-05	0	5	4000000
E	10582	11000	11430	5.00E-05	0	5	4000000

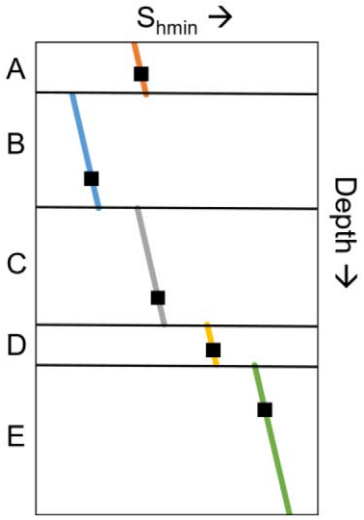

Figure 1—Stress layering considered for the study. The black squares correspond to S_{hmin} interpreted from DFIT measurements conducted at different depths in the wellbore and the lines correspond to the S_{hmin} gradient assumed in the model.

The aim of the operator is to efficiently stimulate and place proppant in Layer D, which contains a high concentration of organic matter. In the simulations we consider that the horizontal section is placed and completed entirely in Layer D. The models represent stimulation on a single plug-and-perf stage of a horizontal well with the following common features in all the simulations:

1. The completion design consists of four perforation clusters with a 50 ft. spacing.
2. There are 12 perforations per cluster.
3. The stimulation is performed with injection of slickwater at a specified flow rate for 2.5 hours, which is varied in the sensitivities.
4. The injection fluid has a specified concentration of proppant for each sensitivity which consists of equal amounts of 40 mesh, 55 mesh and 70 mesh proppant.

Modeling Methodology

The simulations were performed using ResFrac, a 3-D, fully integrated fluid flow and hydraulic fracture propagation code. The simulator is described in detail by McClure and Kang (2018). Fluid flow is modeled by a fully implicit finite volume method. Fracture elements are meshed as rectangles, matrix elements as cuboids, and wellbore elements as line-segments. Fracture propagation is modeled using linear elastic fracture mechanics. Fractures are assumed to propagate linearly (without turning). Following Delaney et al. (1986) and Scholz (2010), fracture toughness is assumed to increase with the square root of the effective fracture length. The stress shadows induced by mechanical fracture opening are calculated by the displacement discontinuity method of Shou et al. (1997) assuming the fracture to be embedded in a homogenous linear elastic medium. The fracture fluid flow is modelled by using general constitutive equations that consider Darcy and non-Darcy flow, Newtonian and non-Newtonian fluids and multiphase flow. Fractures are mechanically open when fluid pressure exceeds the normal stress and the walls go out of contact. Fractures retain aperture and conductivity when mechanically closed. The flow equations for fractures enable smooth transition between limiting cases such mechanically open or closed, propped or unpropped. The conductivity of unpropped fracture elements is lower and more stress sensitive than propped fracture elements. Proppant transport is modelled taking into account proppant grain size, proppant density, fluid viscosity, non-Newtonian rheology, gravitational convection, hindered settling, clustered settling and the effect of proppant on slurry viscosity.

The perforation pressure drop is modelled using the equation (Cramer 1987; Veatch 1983)

$$\Delta P_{pf} = \frac{0.808\, Q^2 \rho}{C_{pf}^2 N_{pf}^2 D_{pf}^4}$$

where Q is the volumetric flow rate, N_{pf} is the number of perforations in the cluster, D_{pf} is the diameter of the perforations and C_{pf} is the coefficient of discharge. The 0.808 factor is for consistent units, it can be computed accordingly for field units.

Results and Discussion

Reference Case

The base case is simulated with a flow rate of 50 bbl/min, 0.32 inches perforation diameter, 1 ppg proppant concentration with the well located 15 ft. from the bottom of layer D. This represents a stimulation stage with 6000 barrels of fluid and 252,000 lbs of proppant. This case is used as the reference case in all the sensitivity analyses.

Figure 2 shows cross-sectional views of the hydraulic fractures propagating from the four perforation clusters. The hydraulic fracture cross-section on the left corresponds to the perforation cluster closest to the toe of the well. Each cross-section represents the hydraulic fracture after two weeks of shut-in following the stimulation, which allows enough time for proppant settling. The color indicates hydraulic fracture conductivity in md-ft which is dominantly controlled by proppant distribution within the fracture and the effective normal stress. The logarithmic color scale highlights the portions of the fracture which contain significant proppant in red. The fracture conductivity in these zones is two orders of magnitude higher than the unpropped portions. The hydraulic fracture conductivity within the unpropped zones is a function of the effective normal stress, which can be observed by the lower conductivities in the unpropped portions of Layer C (green) compared to Layer B (yellow). The unpropped conductivities are similar to the values reported by Zhang et al. (2015) and Wang and Sharma (2018) for similar effective normal stresses. The stress layering is highlighted in the left part of Figure 2 showing the stress gradients within each layer separated by discontinuities at layer boundaries. The relative organic content of the layers is shown on the right part with Layer D having by far the most organic content and is therefore the main target for the operator.

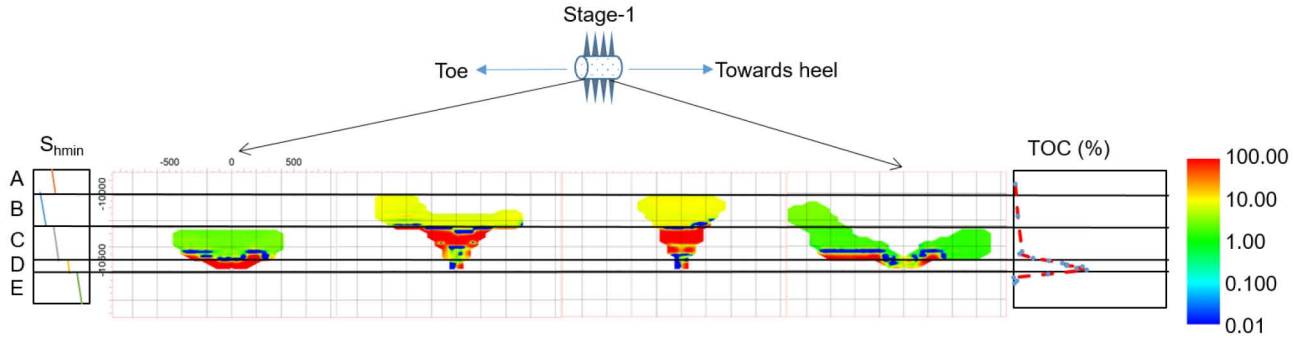

Figure 2—The reference case model showing the hydraulic fracture cross-sections after 2 weeks of shut-in following the stimulation. The figure on the left is the fracture closest to the toe of the well while the figure to the right is the fracture closest to the heel of the well. The left panel shows the S_{hmin} variation in the different layers and the right panel shows the Total Organic Carbon percentage measured from core samples. The logarithmic color scale shows hydraulic fracture conducivity in md-ft with conductivity in the propped zones (red) about two orders of magnitude higher than the unpropped zones.

The dominant trend of the hydraulic fracture growth as seen in Figure 2 is an overall upward propagation with decreasing S_{hmin} above Layer D. Layers A and E act as strong stress barriers due to their high S_{hmin}. The

fracture shapes are influenced by the stress shadow effect which is highlighted by the limited length of the inner fractures in layers C and D and outward growth in layer B.

The stress contrast between the layers affects both the overall fracture geometry and the proppant distribution within the fracture. There is very limited lateral fracture growth and proppant distribution in Layer D with the exception of the toe fracture. Most of the proppant is placed in Layer C, which has relatively less organic content.

Pinch-points

The proppant distribution is controlled by the creation of pinch-points within the fracture. During the injection, the fluid pressure distribution within the fracture is limited by the fracture propagation pressure and hence the S_{hmin} in each individual layer. Due to the stress stratigraphy, this causes significant pressure variations to develop within the crack. The pressure variations can only exist within the high conductivity, open fracture if pinch-points develop. These pinch-points appear as zones of lower aperture and hence lower conductivity associated with the stress boundaries. Figure 3a and Figure 3b show the aperture and pressure distribution within one of the inner fractures in the reference case during the injection period after about 1 hour and 45 minutes into the simulation. The fluid pressure within the fracture is a few 100 psi lower in layer B compared to layer C and D. The pink areas in Figure 3a denote the low aperture and hence low conductivity zones within the fracture at the boundaries of the stress layers. After the end of pumping the fracture closure happens earlier in the higher stress layer D compared to layer C and B. Figure 4 shows the aperture (in inches) for the four hydraulic fractures in Figure 12, a few hours after the end of pumping. It is evident that the aperture starts to close at a much faster rate in the higher stress layers. Depending on the relative diameter of the proppant, the pinch-points have the potential to screen proppant flow. In the current simulation, not much proppant is able to enter Layer B in spite of the high aperture as the pinch-points create a barrier to upward flow. These pinch-points also create barriers to the gravity settling of proppant into layer D and lead to the inefficient proppant distribution in the target layer, creating areas of low hydraulic conductivity between the wellbore and the well propped portions of the fractures.

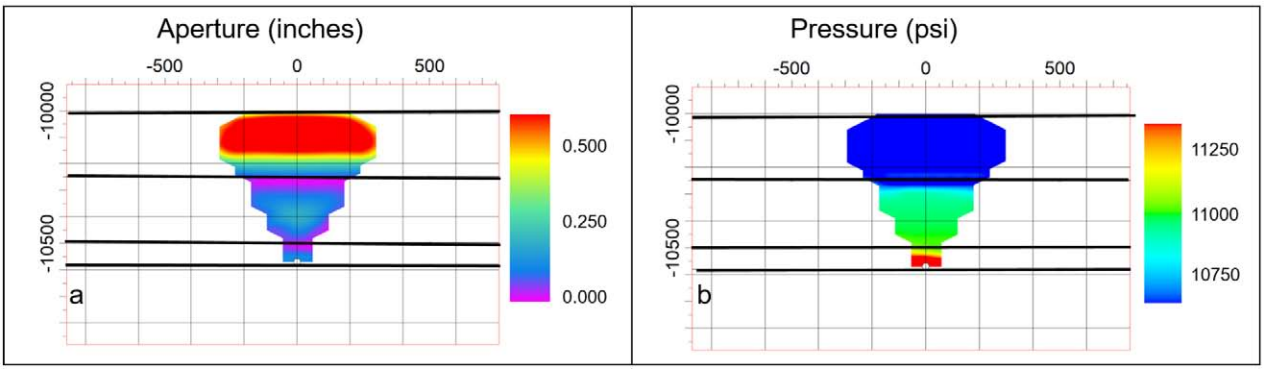

Figure 3—The reference case model showing a) fracture aperture and b) fluid pressure distribution within the fracture after about 1 hour and 45 minutes of pumping. The thick lines denote the stress layer boundaries as in Figure 2. Note the low aperture pinch-points (in pink) close to layer boundaries that enable the existence of a pressure difference of a few 100 psi within the open fracture.

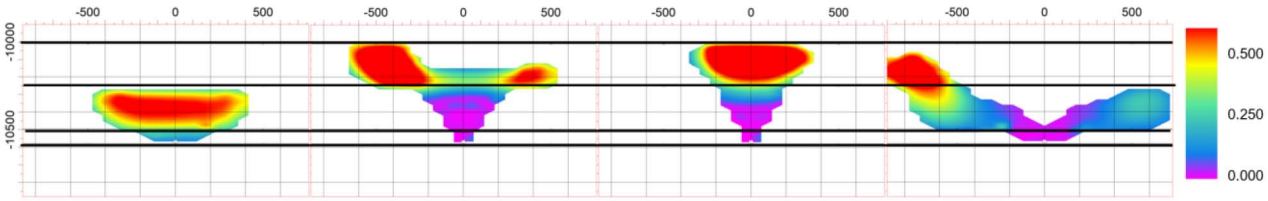

Figure 4—The reference case model showing the fracture aperture in inches at about 10 hours into the simulation. The thick lines denote the layer boundaries as in Figure 2. The fracture appears to close early in the high S_{hmin} layers compared to the lower S_{hmin} layers.

Sensitivity Analysis

Figure 5a, 5b and 5c show the sensitivity analysis of the hydraulic fracture configuration with variation in landing zone, perforation diameter and proppant concentration. The top row of each plot shows the reference case results as shown in Figure 2 for comparison.

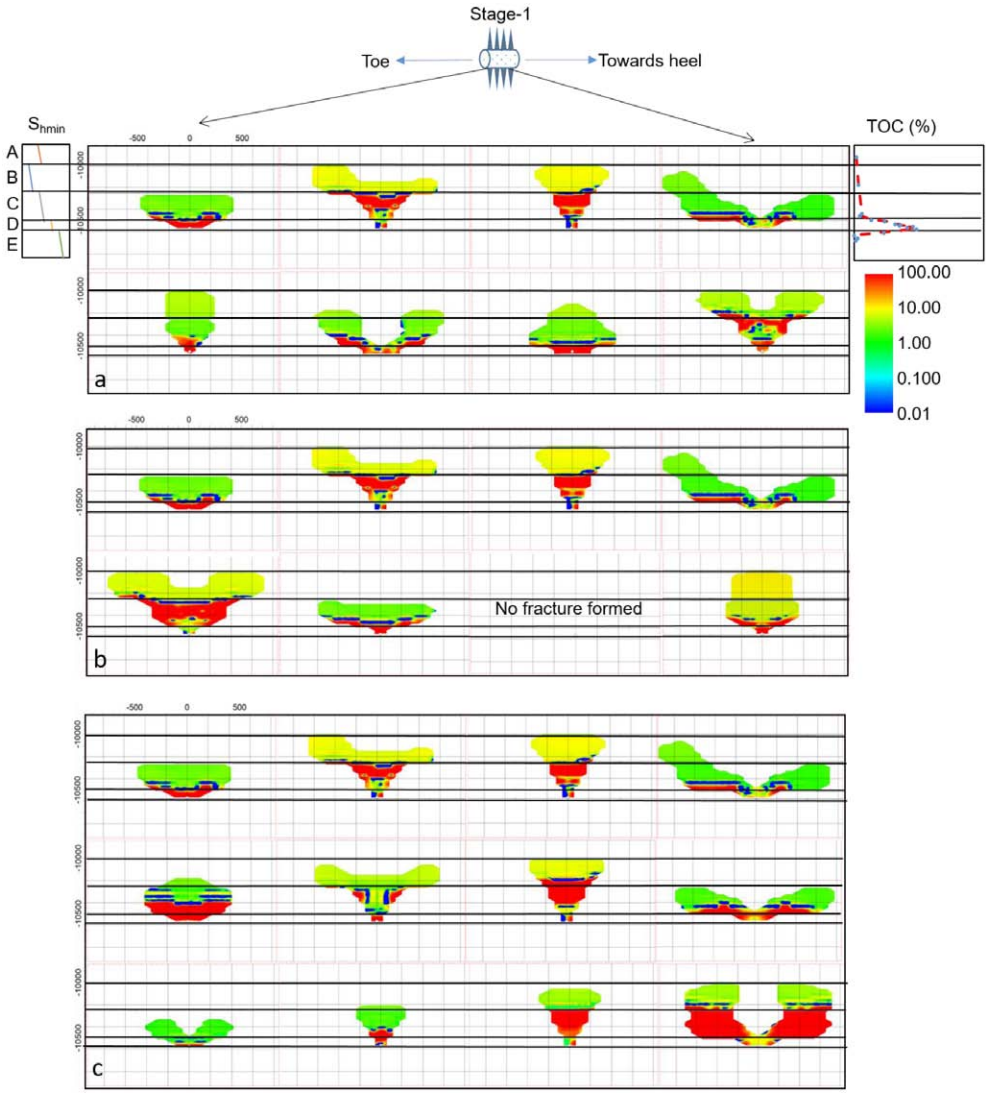

Figure 5—Comparison of the reference case with sensitivities in operational parameters with the same setup as Figure 2. The results are again shown at the end of two weeks of shut-in follwing the stimulation with the colors indicating hydraulic fracture conductivity. The top row of each figure shows the reference case from Figure 2 for comparison. The sensitivities shown are: a) Well placement: The bottom row compares the results with the well placed at the middle of layer D instead of the bottom in the reference case; b) Perforation diameter: The bottom row shows the results with the perforation diameter doubled to 0.64 inches compared to 0.32 inches in the reference case; c) Proppant concentration: The two bottom rows show the results with 3 ppg and 5 ppg proppant concentrations respectively compared to 1 ppg in the reference case.

The lower row of Figure 5a shows the results with the same parameters as in the reference case except that the well is positioned in the middle of Layer D rather than the bottom. This case shows relatively more proppant placement in Layer D for the two inner fractures compared to the reference case

Figure 5b compares the results with a perforation diameter of 0.64 inches in the lower row with the reference case diameter of 0.32 inches in the upper row. The overall pattern of upward hydraulic fracture propagation and low proppant in Layer D remains unchanged. In this case, only the outer two perforation clusters are able to form significant hydraulic fractures. One of the inner clusters has a hydraulic fracture with a limited extent, while one of the clusters is unable to initiate a hydraulic fracture. This is due to the lower perforation pressure drop, which is inversely proportional to the fourth power of the perforation diameter. This leads to the stress shadow effect dominating and the outer two clusters taking almost all the injected fluid.

Figure 5c compares hydraulic fracture propagation with different proppant concentrations. The top row is the reference case of 1 ppg, the middle row utilizes 3 ppg and the bottom row utilizes 5 ppg. The propped area in Layer D is not significantly different in the three cases. The 3 ppg case appears to have the best results visually, while in case of the 5 ppg a massive heel fracture appears to have a placed significant amount of proppant in Layer C.

Figure 6 shows the sensitivities with injection rate. Figure 6a compares the reference case in the top row with an increased injection rate of 100 bbl/min. Note that since the proppant concentration is the same in both cases, the higher injection rate has twice as much proppant and fluid. The higher flow rate aggravates the problem of upward fracture propagation with very little improvement in proppant placement in Layer D.

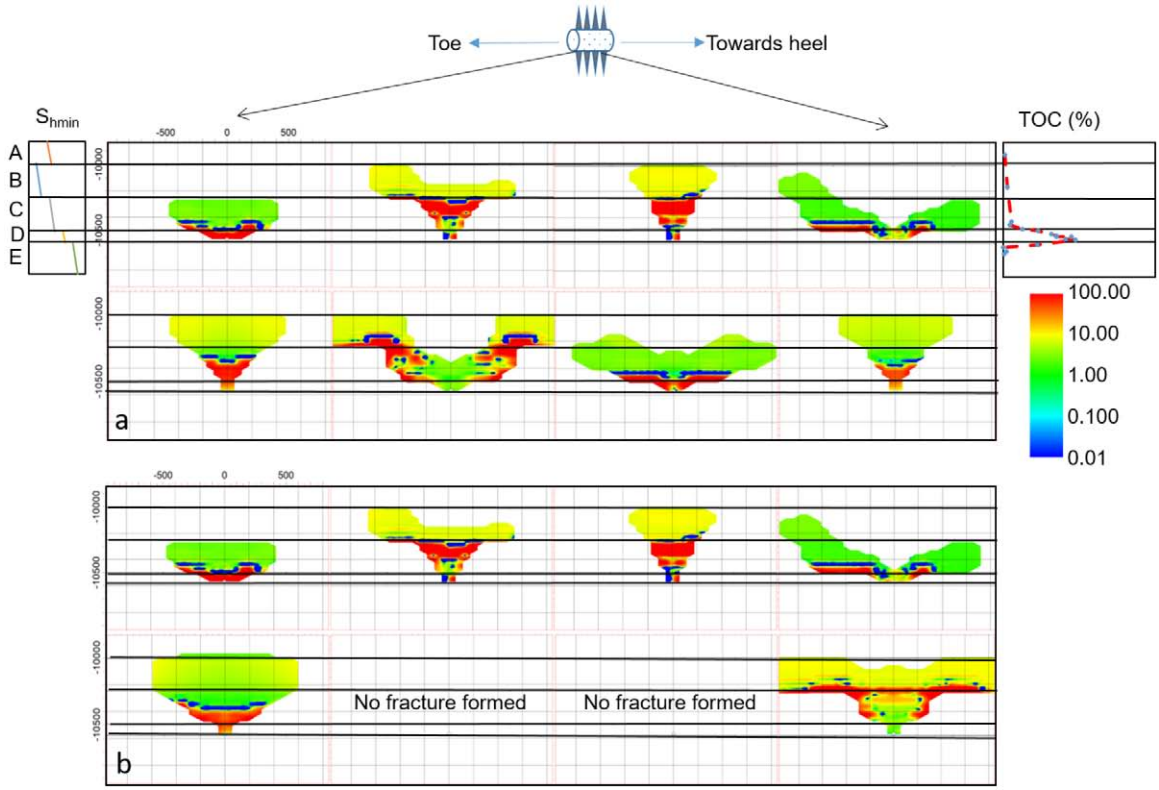

Figure 6—Two additional sensitivies are shown here in the same pattern as Figure 5. The sensitivities shown are: a) Flow rate: The bottom row compares the results with increase in flow rate to 100 bbl/min compared to 50 bbl/min in the reference case; b) Flow rate and perforation diameter: The bottom row shows the results when both the flow rate and the perforation diameter are doubled to 100 bbl/min and 0.64 inches.

Figure 6b compares the reference case in the top row with a combination of an increased flow rate of 100 bbl/min and an increased perforation diameter of 0.64 inches. For this combination, the lower perforation

pressure drop and the higher stress shadows cause an unequal fluid distribution between the clusters with hydraulic fractures forming only the two outer perforation clusters. In addition, there is a higher upward fracture propagation tendency with a high outward growth in layer B.

Figure 7 shows the cumulative normalized gas production over a 5 year period for all the cases. The volumes are normalized with respect to the reference case. Figure 7a compares production from the reference case having the well at the bottom of layer D with the well placement at the middle and top of layer D. The well in the middle shows highest cumulative gas production with the well at top being the worst case. Figure 7b shows the results for the proppant concentration sensitivity. The 5 ppg proppant case clearly yields the highest production.

Figure 7c compares the production from the reference case with increasing the diameter of the perforations, increasing the flow rate and increasing both the diameter of the perforations and the flow rate. There is a 20% increase in production when the flow rate is doubled with the 0.32 inches perforation diameter. Note that since the proppant concentration in the fluid is held fixed the total amount of proppant pumped is also double in this case. The other two cases result in less production. This is because all the perforation clusters are not able to propagate hydraulic fractures for the higher perforation diameter.

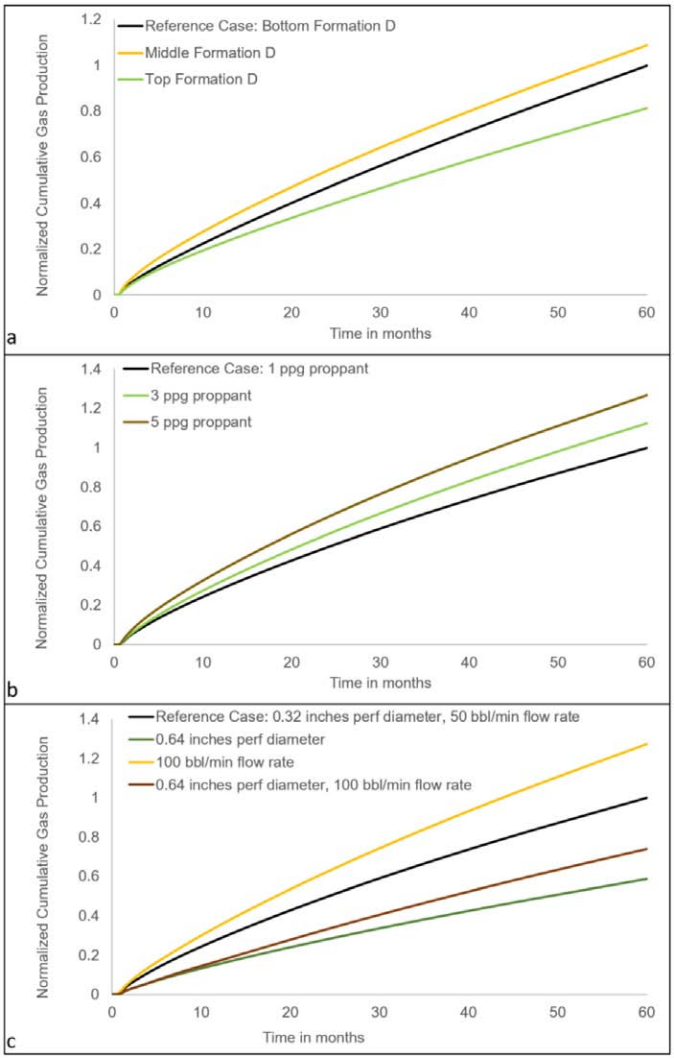

Figure 7—Cumulative production normalized to the reference case is shown for a period of 5 years. The top panel compares the cumulative production for the different well positions. The center panel shows the cumulative production comparison with different proppant concentrations. The bottom panel shows the cumulative production comparison for perforation diameter and flow rate sensitivities.

Stress gradient within the layers vs. constant stress assumption

Stress magnitudes are generally known to increase with depth and therefore use of a slight S_{hmin} gradient within each layer seems to be a reasonable assumption. However, it is not uncommon for models to assume a constant S_{hmin} per layer. A sensitivity of stress gradients is shown in Figure 8, which tests the difference between the two assumptions. The lower row of Figure 8 compares the fracture configuration with a *stair-step* constant S_{hmin} per layer model with the reference case model. The S_{hmin} with depth in both cases is shown on the left side of the rows in Figure 8. Since the stress measurements were made close to the center of the layers, using a constant S_{hmin} per layer increases the stress contrast at the layer boundaries compared to the reference case. There seem to be some differences in the hydraulic fracture configurations in the two cases, however the overall trends of upward fracture propagation, limited lateral extent, sparse proppant placement in layer D and the influence of pinch-points remain unchanged.

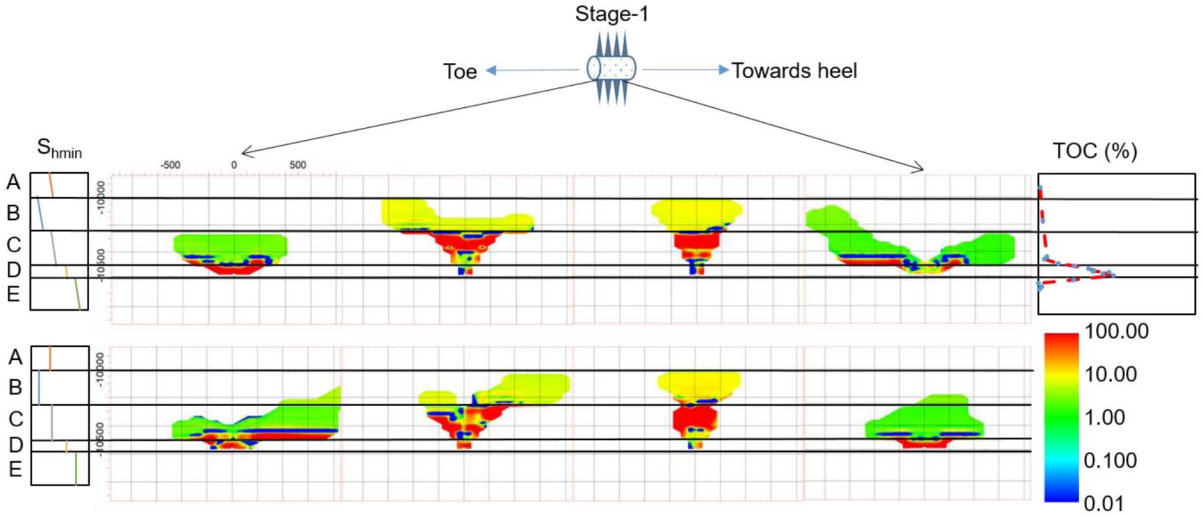

Figure 8—The comparison between the reference case model assuming stress gradients within each layer (top row) vs. a model assuming a *stair-step or blocked* constant S_{hmin} per layer (bottom row). The left hand panels show the stress profile in both cases.

Figure 9 shows the 5 year cumulative gas production for the two cases. The cumulative gas production has a negligible difference in the two cases. This shows that the overall upward fracture growth and proppant placement in the shallower layers, is not a consequence of the representation of stress in the model, rather it is driven by the measured S_{hmin} values in the layers.

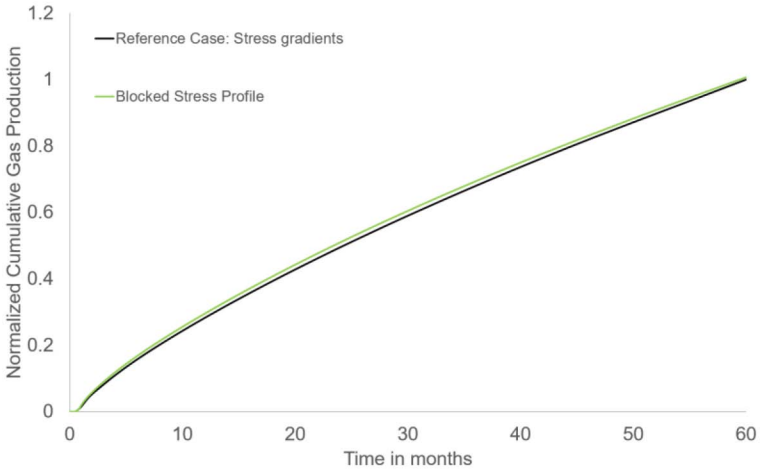

Figure 9—The normalized cumulative gas production over five years for the two cases shown in Figure 8. The green curve shows the production in the *stair-step or blocked* constant S_{hmin} per layer model which is very smiliar to the production in the reference case.

Limitations

The modeling presented above demonstrates the large scale effects of stress layering on hydraulic fracture propagation and are presented to be broadly applicable for the area where the geomechanical model was made. This said, the simulations should be considered recognizing that there are many complexities that play a significant role in hydraulic fracture propagation and proppant placement that are not included in the models and there are number of simplifications in these models such as homogenous permeability, absence of significant natural fracture systems and poroelastic effects which can be tested in future studies. Additionally, recent core through hydraulic fracture studies in the Eagleford and Wolfcamp formations have highlighted a number of surprising results such as the propagations of multiple hydraulic fractures in close proximity and common occurrence of branching fractures (Gale et al. 2018; Raterman et al. 2017). This phenomena is not currently sufficiently understood to be incorporated into the models.

Conclusions

The result of the three dimensional coupling between the vertical variations of S_{hmin}, stress shadows and operational parameters can be complex and non-intuitive. The sensitivities demonstrate the importance of 3-D modelling the integrated effects of well-bore and hydraulic fracture physics with an accurate stress stratigraphy.

The simulations demonstrate the importance of a well-characterized stress state as an input into a stimulation design. The stress contrast determines the overall fracture geometry and the proppant distribution within the fracture. The overall trend in the studied case is upward fracture growth driven by the stress stratigraphy with very little lateral fracture growth and proppant distribution in Layer D, which is the target of the operator.

While microseismic monitoring can be used to constrain the overall facture geometry, the extent of the propped fracture is hard to constrain and areas of high proppant concentrations are often assumed to be in the vicinity of the well. However, the models demonstrate a realization where that need not be the case. The pinch-points observed in all of the simulations are created due to subtle interactions between the fluid flow within the fracture and the stress contrasts in the propagating layer, which creates a high differential pressure within the crack. The high pressure difference can only be sustained due to presence of pinch-points at the boundaries of stress layers. After the end of injection the fracture closes more rapidly in the high stress layer D compared to the lower stress layers B and C. This creates barrier to proppant settling

leading to isolated pockets of high conductivity close to the layer boundaries. In such cases, constraints on the unpropped fracture conductivity are important in predicting the production.

The sensitivities test the effects of design parameter such as landing zone, cluster spacing, perforation diameter, flow rate and proppant concentration. The stress shadow effect tends to promote growth of the outer fractures at the expense of the inner ones for single isolated stages, while the competing perforation pressure drop tends to distribute fluid equally between the perforation clusters. Perforation diameter and flow rate can be adjusted to ensure that the perforation pressure drop is sufficient to overcome stress shadowing and ensure hydraulic fracture propagation from all the perforation clusters. Lower perforation diameter and higher flow rate helps in distributing the flow uniformly and lead to higher volumes of gas produced. Weddle et al. (2018) discuss the role of additional effects such as perforation erosion, well bore friction variations in the completion design to ensure adequate perforation pressure drop.

Nonetheless, it is clear that obtaining stress measurements at different depths and investigating the sensitivity of stimulation to a variety of operational parameters are strongly recommended in order to optimize the stimulation design. Sensitivity analysis with different configurations of the stress layering to test the interaction between geological uncertainties and stimulation design is recommended to visualize the entire spectrum of uncertainties in hydraulic fracture propagation and proppant placement. The diagnostic plots used in this study are an effective way of visualizing the stimulation process.

References

Agarwal, Karn, Michael J. Mayerhofer, and Norman Raymond Warpinski. 2012. "Impact of Geomechanics on Microseismicity." In SPE/EAGE European Unconventional Resources Conference and Exhibition. Society of Petroleum Engineers. https://doi.org/10.2118/152835-MS.

Alalli, Abdulgader A., and Mark D. Zoback. 2018. "Microseismic Evidence for Horizontal Hydraulic Fractures in the Marcellus Shale, Southeastern West Virginia." *The Leading Edge* **37** (5). Society of Exploration Geophysicists : 356–61. https://doi.org/10.1190/tle37050356.1.

Cramer, D.D. 1987. "The Application of Limited-Entry Techniques in Massive Hydraulic Fracturing Treatments." *SPE Production Operations Symposium*. https://doi.org/10.1007/s00228-012-1234-5.

Daneshy, Ali Ali. 2014. "Fracture Shadowing: Theory, Applications and Implications." In SPE Annual Technical Conference and Exhibition. Society of Petroleum Engineers. https://doi.org/10.2118/170611-MS.

Delaney, Paul T., David D. Pollard, Joseph I. Ziony, and Edwin H. McKee. 1986. "Field Relations between Dikes and Joints: Emplacement Processes and Paleostress Analysis." *Journal of Geophysical Research* **91** (B5): 4920. https://doi.org/10.1029/JB091iB05p04920.

Fisher, M. Kevin, and Norman R. Warpinski. 2012. "Hydraulic-Fracture-Height Growth: Real Data." *SPE Production & Operations* **27** (01): 8–19. https://doi.org/10.2118/145949-PA.

Fisher, M.K., J.R. Heinze, C.D. Harris, B.M. Davidson, C.A. Wright, and K.P. Dunn. 2004. "Optimizing Horizontal Completion Techniques in the Barnett Shale Using Microseismic Fracture Mapping." In SPE Annual Technical Conference and Exhibition. Society of Petroleum Engineers. https://doi.org/10.2118/90051-MS.

Gale, Julia F. W., Sara J. Elliott, and Stephen E. Laubach. 2018. "Hydraulic Fractures in Core From Stimulated Reservoirs: Core Fracture Description of HFTS Slant Core, Midland Basin, West Texas." Proceedings of the 6th Unconventional Resources Technology Conference, no. 1993. https://doi.org/10.15530/urtec-2018-2902624.

Ma, Xiaodong, and Mark D. Zoback. 2017. "Lithology-Controlled Stress Variations and Pad-Scale Faults: A Case Study of Hydraulic Fracturing in the Woodford Shale, Oklahoma." *Geophysics* **82** (6): ID35–ID44. https://doi.org/10.1190/geo2017-0044.1.

McClure, Mark, and Charles Kang. 2018. "ResFrac Technical Writeup," April. http://arxiv.org/abs/1804.02092.

Miskimins, Jennifer, Bill E. Wheaton, Daniel Wood, Trey Lowe, and Robert Barree. 2014. "Integration of Distributed Temperature and Distributed Acoustic Survey Results with Hydraulic Fracture Modeling: A Case Study in the Woodford Shale." In Proceedings of the 2nd Unconventional Resources Technology Conference, 1–14. Tulsa, OK, USA: American Association of Petroleum Geologists. https://doi.org/10.15530/urtec-2014-1922140.

Raterman, Kevin T., Helen E. Farrell, Oscar S. Mora, Aaron L. Janssen, Seth Busetti, Jamie McEwan, Baishali Roy, et al. 2017. "Sampling a Stimulated Rock Volume: An Eagle Ford Example." In Proceedings of the 5th Unconventional Resources Technology Conference. Tulsa, OK, USA: American Association of Petroleum Geologists. https://doi.org/10.15530/urtec-2017-2670034.

Scholz, Christopher H. 2010. "A Note on the Scaling Relations for Opening Mode Fractures in Rock." *Journal of Structural Geology* **32** (10). Elsevier Ltd: 1485–87. https://doi.org/10.1016/j.jsg.2010.09.007.

Shou, Keh-Jian, Eduard Siebrits, and Steven L. Crouch. 1997. "A Higher Order Displacement Discontinuity Method for Three-Dimensional Elastostatic Problems." *International Journal of Rock Mechanics and Mining Sciences* **34** (2). Pergamon: 317–22. https://doi.org/10.1016/S0148-9062(96)00052-6.

Soliman, Mohamed Y., Loyd E. East, and David Lee Adams. 2008. "Geomechanics Aspects of Multiple Fracturing of Horizontal and Vertical Wells." *SPE Drilling & Completion* **23** (03). Society of Petroleum Engineers: 217–28. https://doi.org/10.2118/86992-PA.

Veatch, R W. 1983. "Overview of Current Hydraulic Fracturing Design and Treatment Technology-Part 2." *Journal of Petroleum Technology* **35** (5): 853–64. https://doi.org/10.2118/10039-PA.

Wang, HanYi, and Mukul M. Sharma. 2018. "Estimating Unpropped Fracture Conductivity and Compliance from Diagnostic Fracture Injection Tests." In SPE Hydraulic Fracturing Technology Conference and Exhibition. Society of Petroleum Engineers. https://doi.org/10.2118/189844-MS.

Warpinski, Norman R., Michael Mayerhofer, Karn Agarwal, and Jing Du. 2013. "Hydraulic-Fracture Geomechanics and Microseismic-Source Mechanisms." *SPE Journal* **18** (04). Society of Petroleum Engineers: 766–80. https://doi.org/10.2118/158935-PA.

Warpinski, Norman R., Paul Branagan, and Roy Wilmer. 1985. "In-Situ Stress Measurements at U. S. DOE's Multiwell Experiment Site, Mesaverde Group, Rifle, Colorado." *Journal of Petroleum Technology* **37** (3): 527–36. https://doi.org/10.2118/12142-PA.

Weddle, Paul, Larry Griffin, C Mark Pearson, and Liberty Resources. 2018. "SPE-189880-MS Mining the Bakken II-Pushing the Envelope with Extreme Limited Entry Perforating." https://www.onepetro.org/download/conference-paper/SPE-189880-MS?id=conference-paper%2FSPE-189880-MS.

Xu, Shaochuan, and Mark D. Zoback. 2015. "Analysis of Stress Variations with Depth in the Permian Basin Spraberry / Dean / Wolfcamp Shale." *American Rock Mechanics Association* 15–189.

Zhang, Junjing, Anton Kamenov, D. Zhu, and A. D. Hill. 2015. "Measurement of Realistic Fracture Conductivity in the Barnett Shale." *Journal of Unconventional Oil and Gas Resources* **11**. Elsevier Ltd: 44–52. https://doi.org/10.1016/j.juogr.2015.05.002.